IGF9 IX Convegno Nazionale
Gruppo Italiano Frattura
Roma, 2-4 giugno 1993

DEFORMATION AND FAILURE OF HIGH TEMPERATURE METAL MATRIX COMPOSITES

Golam M. Newaz
Battelle Memorial Institute
Columbus, Ohio, U.S.A.

ABSTRACT

Inelastic deformation mechanisms under monotonic tension, compression, tension-tension fatigue and, thermomechanical fatigue loading in titanium-based metal matrix composites considered for high temperature applications are presented. It is observed through rigorous experimental evaluation that the inelastic deformation mechanisms such as microcracking, debonding, matrix plasticity and fiber fracture contribute to failure of the unidirectional composites in various ways for various loading modes.

Because of the significant differences in inelastic deformation mechanisms under monotonic tension (primarily matrix plasticity) and fatigue (primarily fiber-matrix debonding and matrix crack growth), it is difficult to extend the constitutive model developed for monotonic loading to be applicable for fatigue conditions. It is suggested that because of the current deficiencies in constitutive and life models, rational models should be developed in the future which couples plasticity and damage. Furthermore, it should consider the differences in damage modes for various type of loading modes, e.g., tension, compression and thermomechanical fatigue.

INTRODUCTION

An important aspect of inelastic deformation characteristics of metal matrix composites (MMC) is that both plasticity and microcracking may be present simultaneously. The role of these inelastic deformation characteristics on the constitutive response of MMC is a major issue. Newaz and Majumdar [1,2] and Majumdar and Newaz [3] have

addressed these issues extensively. The sequence of events at the constituent level need to be critically examined for developing a complete understanding of the constitutive behavior of the composite and for identifying the critical events which affect failure of the composite. From a design perspective, such information are considered important for developing rational failure criteria for MMCs.

In MMCs there is significant difference in the coefficient of thermal expansion between the fiber and the matrix; the matrix has larger coefficient of thermal expansion. Consequently, large compressive radial stresses build up at the interface between the matrix and the fiber as the composite is cooled from the processing temperature. On the other hand, the axial and circumferential stresses in the matrix are both tensile in nature. This combination of stresses set up yielding or near yielding conditions in the matrix immediately adjacent to the fiber. A consequence of such high stresses is that micro-yielding may occur well before macroscopic yield is observed when the MMC is loaded mechanically. In addition, the strength of the bond between the fiber and the matrix has been shown to be weak in the composite by Majumdar and Newaz [3] and Johnson, et al [4]. Also, the presence of reaction zone adds another dimension to the complex deformation characteristics in these composites under applied loading. Considerable work in this field is now underway. Some recent studies show that deformation and failure are of significant interest for MMCs [1-9].

The deformation and failure mode of the MMCs under different loading modes are likely to be different. The individual roles of matrix, interface and the fiber are likely to be different under different loading conditions as well.

In order to determine the role of the constituents on the overall deformation and failure, experimental investigations were conducted for both monotonic and fatigue loading. The following evaluations were conducted: (1) monotonic tensile and compression, (2) isothermal fatigue and (3) thermomechanical fatigue. The deformation and failure characteristics for each of these loading modes were carefully evaluated. The effect of these deformation and failure mechanisms and their implications on life modeling requires special attention. This area is also addressed in this paper.

EXPERIMENTAL ASPECTS

For monotonic tension and compression, the material tested was an 8-ply unidirectional Ti 15-3/SCS-6 composite, approximately 2 mm thick with a fiber volume fraction of approximately 0.34. The SCS-6 (SiC) fiber diameter is approximately 140 micrometers, and it contains alternating outer layers of C and Si, which protect the fiber from damage during handling. The Ti 15-3 alloy is a metastable body centered cubic (bcc) beta Ti-alloy, the bcc phase being stabilized by V. The material is metastable because hexagonal close packed (hcp) alpha phase, which is the stable room-temperature phase

of pure Ti, precipitates when the material is held at temperatures as low as 400 C for long periods of time. The specimen dimensions for tension and compression are given in References 1 and 2.

Specimens were gripped using friction grips, and loaded on a servohydraulic testing machine at a strain rate of approximately 0.002/sec for tension and 0.004/sec in compression. The longitudinal and width strains were measured using extensometers.

The fatigue and thermomechanical fatigue (TMF) tests were conducted using dog bone shaped specimens. The fiber volume fraction in these specimens was 0.15. Room temperature (RT) fatigue tests were conducted. The isothermal fatigue tests were conducted at 538 C. The TMF tests were conducted in argon for 200-538 C temperature cycle. Both in-phase and out-of-phase tests were conducted. All fatigue and TMF tests were conducted for an R-ratio of 0.1.

RESULTS AND DISCUSSION

Monotonic Tension

Loading-Unloading Response

Figure 1 shows the stress-strain response for a 0-degree specimen. Results include three tested specimens from Battelle's data and one from NASA-Lewis. The reproducibility is excellent with non-linear deformation starting at approximately 0.55 percent strain. In Figure 1, specimen 0-9 was partially unloaded from about 0.55 percent strain (point B) and then reloaded to failure. Specimen 0-1 was completely unloaded from a higher value of total strain (point D, 0.8 percent). Calculation of the slopes of the loading and unloading lines indicated that the stiffness of the specimens were essentially constant, with an effective elastic modulus of 176.5 GPa (25.6 Msi). In addition, there were significant strain offsets at zero load when specimens were unloaded from the inelastic regime of deformation. Thus, these results appear to indicate that the primary inelastic deformation mode was plasticity.

Figure 2 illustrates the stress-strain behavior for four 90-degree specimens. Once again, the figure illustrates excellent reproducibility of the stress-strain response. The 90-degree specimens show a characteristic 3-stage behavior. The initial elastic modulus was 111 GPa (16.1 Msi). The 90-20 specimen shows a bilinear unloading response in stage II when unloaded from a strain level of 0.5 percent strain.

The unloading slope is approximately 43 percent less than the loading stiffness, implying a significant contribution of damage. Although not shown here, additional experiments

with the 90-degree lamina showed that the reloading curves were almost identical with the unloading curves, illustrating the bilinear nature of the stress-strain response.

Poisson's Ratio

Poisson's ratio in structural materials may provide valuable information on the state of damage and plasticity. Plastic deformation is associated with an increase in Poisson's ratio with fully plastic conditions occurring at a Poisson's ratio of 0.5. If damage occurs in a material due to microcracks, Poisson's ratio will decrease.

Plots of Poisson's ratio (Figures 3 and 4) for both 0 and 90 degree specimens show that the Poisson's ratio slightly increases for the 0-degree and decreases almost to zero for the 90-degree specimen. This confirms that deformation in the 0-degree specimen is primarily due to plasticity, and that of the 90-degree specimen is dominated by damage in the form of fiber-matrix debonding. Note that in the 90-degree lamina, even elastic-plastic calculations indicate that the Poisson's ratio should decrease with inelasticity. However, the decreases that were observed were substantially larger than any that would be predicted without incorporating damage.

Microstructural Evaluation

Monotonic Tension:

In-situ examination of specimens using the replication technique and microscopy of specimens unloaded from different strains provided information on the evolution of damage and plasticity, and their role on the final failure of the composites. The sequence of deformation mechanisms are summarized in Tables 1 and 2 for the 0-degree and 90-degree specimens, respectively. Detailed information can be found in reference [1].

Monotonic Compression

Mechanical Behavior

The typical stress-strain response including unloading for a $[0]_8$ specimen is shown in Figure 5. The compression test result without buckling guides is also shown in the same figure. The elastic modulus in tension and compression were similar, ranging between 175-179 GPa. Also, the corresponding tension data is presented in the same plot. It may be noted that the compression capability of the $[0]_8$ lamina is significantly higher than the tension case both in terms of (1) the onset of nonlinearity and (2) the higher ultimate strength (when premature buckling is avoided). The compression specimen was not loaded to failure. However, experimental efforts suggest that the compression strength will be quite high. In the absence of restraint for buckling, it is

clear that premature buckling takes place resulting in no useful information in the nonlinear deformation regime. The failure mode for compression without buckling guides will be discussed in the Microstructural Evaluation section. The unloading line is parallel to the elastic loading line for the $[0]_8$ composite and indicate that the deformation response is controlled primarily by plastic deformation.

Figure 6 shows the typical stress-strain response of the $[90]_8$ lamina for the three different temperatures, namely, room temperature, 538°C (1000°F) and 650°C (1200°F). In each case, the specimens were unloaded in the nonlinear regime. There is a progressive loss in elastic modulus and proportional limit as a function of temperature as given in Table 3. The distinct knee observed in tension for the onset of nonlinearity in the $[90]_8$ lamina is clearly absent in the case of compression. The onset of nonlinearity in the tension stress-strain curve was attributed to fiber-matrix debonding - a dominant damage mechanism for the $[90]_8$ MMC lamina. Note the large work hardening period for the MMC, extending from approximately 0.5 percent strain to approximately 1 percent strain. This period was much longer then for the matrix material.

Microstructural Evaluation

Monotonic Compression:

Optical photomicrographs of replicas taken from polished specimens showed the presence of extensive matrix plasticity in the lamina. Fiber-matrix debonding is also evident at higher strain levels within the ply. These observations were only made at room temperature. The failure due to fiber buckling in an unrestrained test is shown in Figure 7. The fibers break in a shear plane within the gage section. This failure is indicative of a buckling instability due to compressive load.

Optical photomicrographs of transverse specimens polished after testing revealed the nature of deformation characteristics under compressive loading quite clearly. The initial deformation mechanism under monotonic compressive loading is found to be matrix plasticity along the loading axis between fibers (Figure 8).

Careful observation also reveals a very interesting damage condition in the transverse MMC lamina compression. There are radial cracks (RC) within the fibers oriented primarily along the compression loading axis which form after the initial slip lines have developed in the matrix as mentioned earlier. Reaction zone cracks (rzc) are also observed. These damage modes are depicted in Figure 8. This damage mode was reported earlier by Newaz and Majumdar [10]. Radial fiber cracking is indicative of the low radial fiber strength which may be related to the soft carbon core in the SCS-6 fiber and the columnar grain structure of the CVD deposited SiC with grain boundary facets oriented radially. These cracks are not observed in as-received materials and were not observed in the tension loading mode. The transverse lamina compression results in terms of mechanisms are presented in Table 3.

Fatigue and Thermomechanical Fatigue

Fatigue behavior in many composite materials exhibit three regimes as shown in Figure 9. Room temperature fatigue results are shown in Figure 10 for 15 vol % SCS-6/Ti 15-3 composite. It may be noted that there is a regime of fatigue degradation (sloping line) in the mid-life regime (Regime II). Damage evolution in the very short life regime and in the mid-life regime were evaluated. It was found that short life was dominated by localized fiber fracture and extensive debonding. At mid-life matrix cracking and debonding were prominent. These are summarized in Table 4.

TMF evaluation showed (Figure 11) that in-phase TMF life is shorter than out-of-phase TMF life. Isothermal stress-life line is also shown in the same plot. Isothermal fatigue at high stresses show fiber-matrix debonding (Figure 12) which is similar to what was observed at RT fatigue at high stresses. Careful investigation of damage mechanisms showed that in-phase TMF failure is dominated by fiber fracture and debonding (Figure 13). Out-of-phase TMF damage mechanism is dominated by matrix microcracking and subsequent matrix crack growth leading to failure (Figure 14).

DISCUSSION

It is quite clear by comparing the deformation mechanisms for various loading conditions (Table 1-4) that there are distinctly different inelastic deformation mechanisms which contribute to the overall failure of the MMC.

Extension of our understanding under tensile monotonic loading cannot be easily made to predict the deformation and failure modes observed under, say, fatigue loading or TMF loading. It is also found that tension and compression loading produce different damage conditions. Therefore, one anticipates quite complex deformation and damage mechanisms to operate in the case of reversed fatigue loading. This understanding has a major implication on life modeling for these composites.

Although, realistic constitutive models can be developed based on idealizing the inelastic deformation mechanisms observed using mechanics principles, modification to these constitutive models will be required to reflect the damage modes in fatigue loading conditions. Without such modifications, local stress or strain may not be accurately calculated for life assessment and prediction. Furthermore, any type of growth law to be formulated will require special attention of the changes in inelastic deformation mechanisms as a function of loading.

It is anticipated that life prediction models for these composites will be quite difficult to formulate in the first place. History of damage accumulation needs to be coupled with

plasticity to develop rational models. Current constitutive models for MMCs are plasticity-based [11]. Also, mechanics of materials approach [12] for constitutive model does not account for plasticity -- which is a serious weakness.

Constitutive models that account for both damage (microcracks) and plasticity should be the starting basis for life models. Finite element analysis which couples damage and plasticity [13] shows promise. Much work needs to be done along this line.

CONCLUSIONS

1. Under monotonic tension, the deformation mechanisms in unidirectional longitudinal MMC is plasticity dominated. Deformation in the transverse MMC lamina is strongly influenced by debonding and plasticity.

2. Under monotonic compression, unidirectional MMC shows extensive plastic deformation and some interfacial damage. Failure of the longitudinal lamina is by buckling instability of the fibers. Transverse MMC shows radial fiber cracking, debonding and matrix plasticity as well. Failure of the transverse MMC lamina is due to shear failure of the matrix.

3. The low cycle fatigue deformation mechanism is controlled by fiber fracture and fiber-matrix debonding. Matrix cracking is prominent at medium life range.

4. For TMF conditions, the fatigue mechanism for in-phase and out-of-phase loading are different. In-Phase TMF shows extensive fiber fracture and interfacial debonding. Fracture for in-phase appears to be due to overload fracture. Out-of-phase TMF shows extensive matrix cracking. Failure for out-of-phase specimen is due to typical fatigue crack extension.

5. Constitutive and life models which reflect both damage and plasticity need to be developed with regard to care of the loading mode.

ACKNOWLEDGEMENT

The author acknowledges the Italian Group of Fracture and the IGF-9 Organizing Committee for extending the invitation to present this paper at IGF-9 meeting. The author is grateful to Professor Mario Marchetti and Dr. Nicholas Bonora of the Aerospace Engineering Department at the University of Rome for their encouragement to participate in the IGF-9 meeting.

REFERENCES

1. Newaz, G. M., Majumdar, B. S., "Deformation and Failure Mechanisms in MMC", AD-22, ASME Winter Annual Meeting, Atlanta, 1991, pp. 55-66.

2. Newaz, G. M., Majumdar, B. S., "Inelastic Deformation Mechanisms in Metal Matrix Composites Under Compression," Final Report to NASA-LeRC, Cleveland, February, 1993.

3. Majumdar, B. S., Newaz, G. M., "Inelastic Deformation in Metal Matrix Composites: Plasticity and Damage Mechanisms", Philosophical Magazine, London, Vol. 66, #2, 187-212, 1992.

4. Johnson, W. S., Lubowinski, S. J., Highsmith, A. L., "Mechanical Characterization of Unnotched SCS-6/Ti-15-3 Metal Matrix Composites at Room Temperature", ASTM STP 1080, pp. 193-218, 1990.

5. Majumdar, B. S., Newaz, G. M., Ellis, J. R., "Evaluation and Damage in Ti Based Fiber Reinforced Composites," to appear in Metall. Trans. (1993).

6. Sun, C. T., "Modeling Continuous Fiber Metal Matrix Composite as an Orthotopic Elastic-Plastic Material", ASTM STP 1032, 1989, pp. 148-160.

7. Lerch, B. A., Saltsman, J. F., "Tensile Deformation Damage in SiC Reinforced Ti-15V-3Cr-3Al-3Sn", NASA Technical Memorandum 103620, April, 1991.

8. Newaz, G. M., Majumdar, B. S., Brust, F. W., "Thermal Cycling Response of Quasi-Isotropic Metal-Matrix Composites", ASME J. of Engg. Materials and Technology, April, 1992, pp. 156-161.

9. Nimmer, R. P., Bankert, R. J., Russell, E. S., Smith, G. A., Wright, K. P., "Micromechanical Modeling of Fiber/Matrix Interface Effects in Transversely Loaded SiC/Ti-6-4 Metal Matrix Composites Technology and Research, V. 13, 1, 1991, pp. 3-13.

10. Newaz, G. M., Majumdar, B. S., "Failure Modes in Transverse MMC Lamina Under Compression," J. of Materials Science and Letters, Vol. 12, 551-552, 1993.

11. Dvorak, G. J., Bahei-El-Din, J. Appl. Mech., V. 49, pp. 327-335, 1982.

12. Chamis, C. C., Hopkins, D. A., "Thermo-Viscoplastic Nonlinear constitutive Relationships for Structural Analysis of High Temperature Metal Matrix Composites," Testing Technology of Metal Matrix Composites, Ed. P. R. Giovanni and N. R. Adsit, ASTM STP 964, pp. 177-196, 1988.

13. Brust, F. W., Majumdar, B. S., Newaz, G. M., "Constitutive Response Analysis of Metal Matrix Composites via the Unit Cell Model," presented at the ASTM Symposium on Composite Materials, Pittsburgh, May, 1992.

TABLE 1. TENSILE DEFORMATION MECHANISMS IN $[0]_8$ SCS-6/Ti 15/3 COMPOSITES

Deformation Mechanisms	Applied Lamina Strain
Nucleation of slip bands at reaction zone cracks	~0.004-0.005
Nucleation of slip bands at grain boundaries—onset of extensive plastic deformation	~0.006
Localized fiber-matrix debonding within fiber coating layers caused by reaction zone cracks	~0.006
Extensive slip band formation in matrix	~0.008
Fiber failure initiated by Mo-ribbon fracture	>0.001

TABLE 2. TENSILE DEFORMATION MECHANISMS IN $[90]_8$ SCS-6/Ti 15/3 COMPOSITES

Deformation Mechanisms	Applied Lamina Strain
Onset of minimal plastic slip bands at the top and bottom of fiber	~0.002
Onset of partial fiber-matrix debonding	~0.003-0.005
Slip bands and reaction zone microcracks around 90° from loading axis	~0.006
Extensive fiber-matrix debonding followed by extensive matrix plasticity	>0.006
Formation of intense shear bands between fibers leading to shear fracture	>0.014

TABLE 3. COMPRESSIVE DEFORMATION MECHANISMS IN $[90]_8$ SCS-6/Ti 15/3 COMPOSITES

Inelastic Deformation Mechanisms	Applied Lamina Strain
Plastic Slip Band	0.002*
Debonding	0.006-0.008
Reaction Zone Cracks	0.006
Radial Fiber Cracking	0.006-0.008
Extensive Matrix Plasticity	>0.01

* Data not retrievable at earlier strain/stress levels because of poor replica.

TABLE 4. FATIGUE DEFORMATION MECHANISMS IN $[0]_8$ LAMINA AT RT

Cyclic Range (No. of Cycles)	Deformation Mechanism
Low Cycles (100-10,000 cycles)	Extensive fiber-matrix debonding and local plastic deformation followed by fiber overload fracture
Intermediate Cycles to High Cycles (>10,000 cycles - 10^6 cycles)	Fiber-matrix debonding, extensive matrix crack growth and fiber fracture

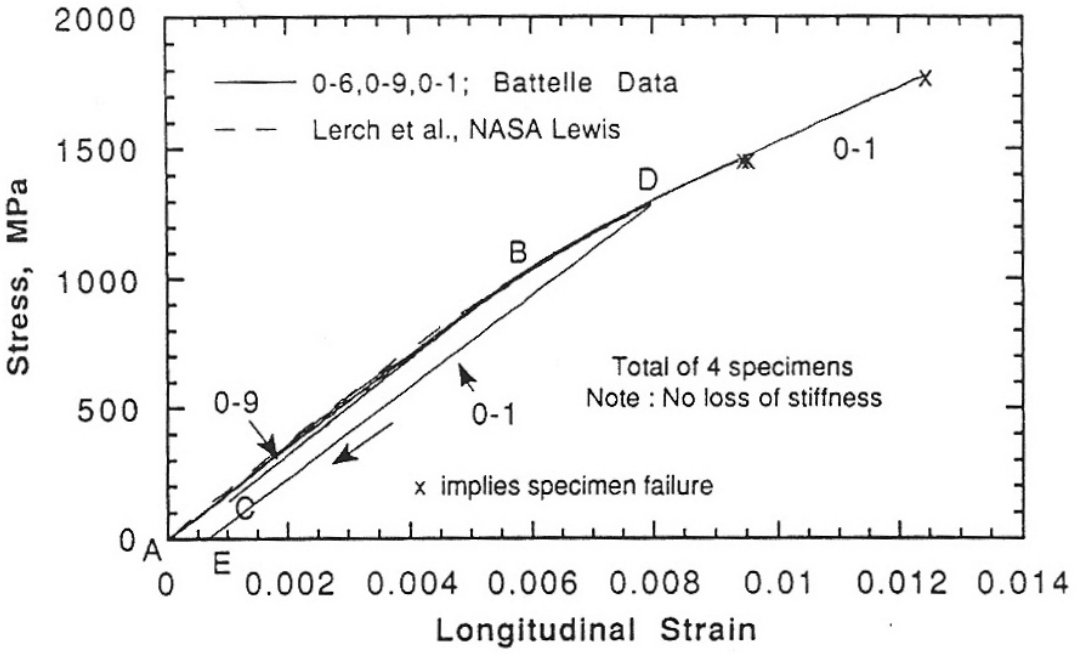

Figure 1. Stress Versus Longitudinal Strain for 0-Degree TI 15-3/SCS-6 Composites

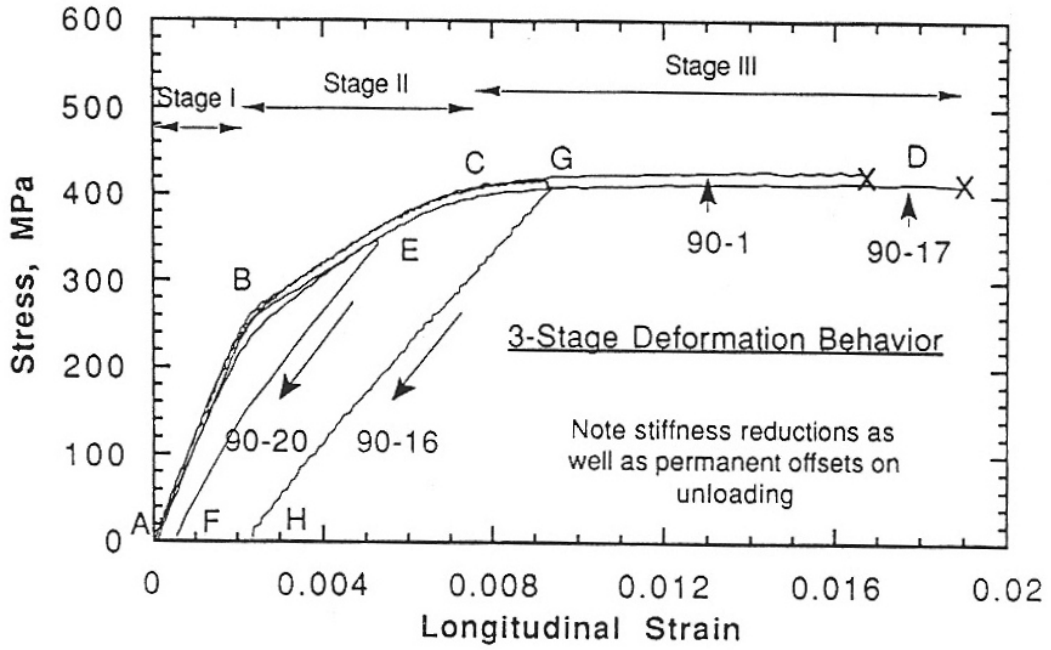

Figure 2. Stress Versus Longitudinal Strain for 90-Degree TI 15-3/SCS-6 Specimens

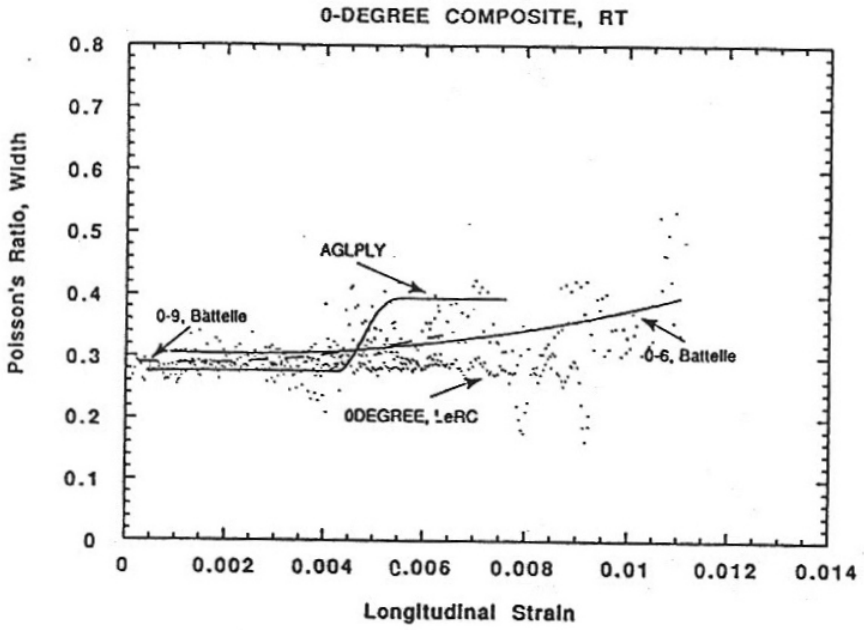

Figure 3. Instantaneous Poisson's ratio in the width direction plotted versus the longitudinal strain for 0-degree specimens; the lines correspond to least-square best-fit polynomials to the data. The results of the AGLPLY analysis is also shown.

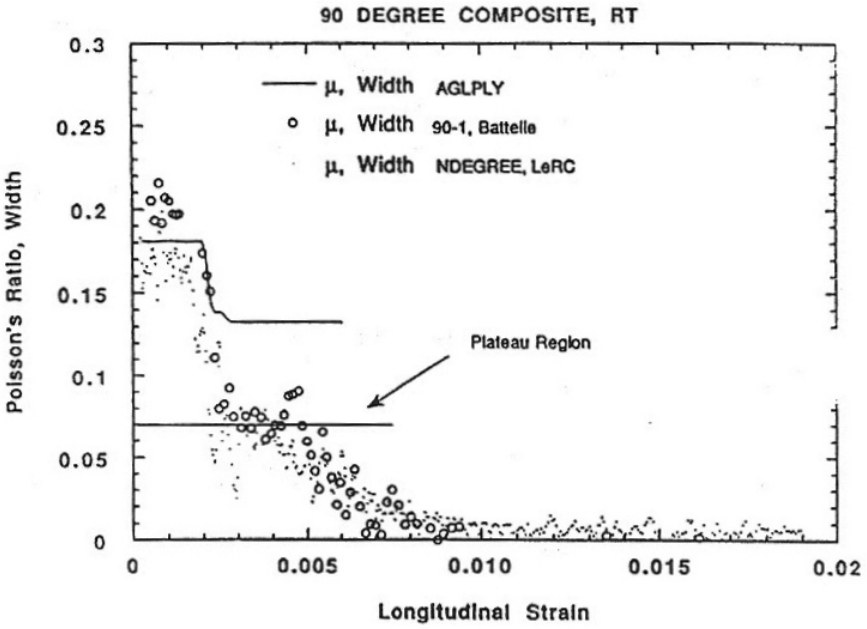

Figure 4. Instantaneous Poisson's ration in the width direction plotted versus the longitudinal strain for 90-degree specimens. The results of the AGLPLY analysis is also shown by the inverted S-shaped curve.

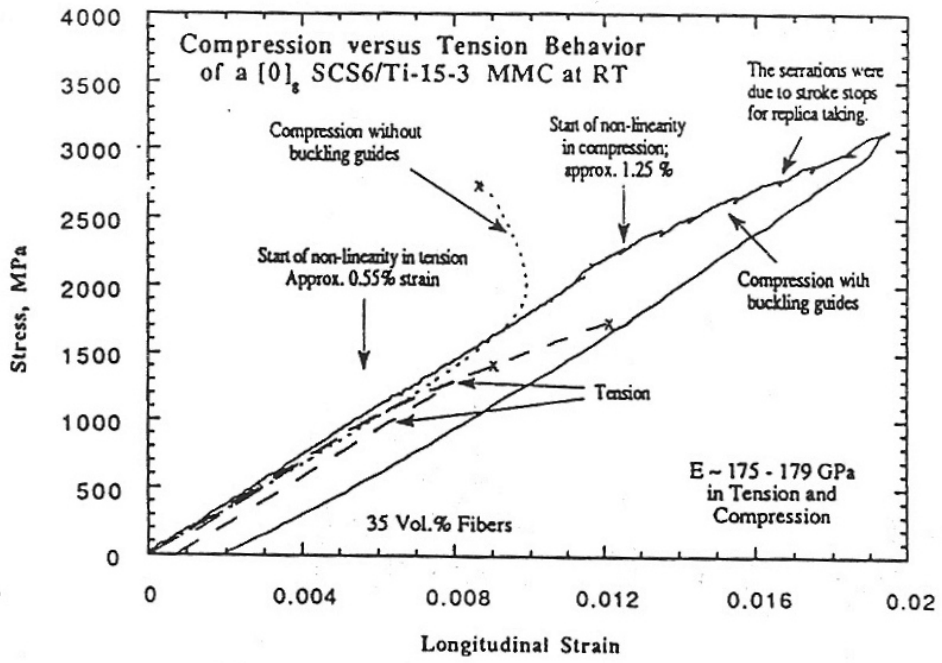

Figure 5. Typical stress-strain response of $[0]_8$ lamina in compression. Also includes tension results for the same lamina.

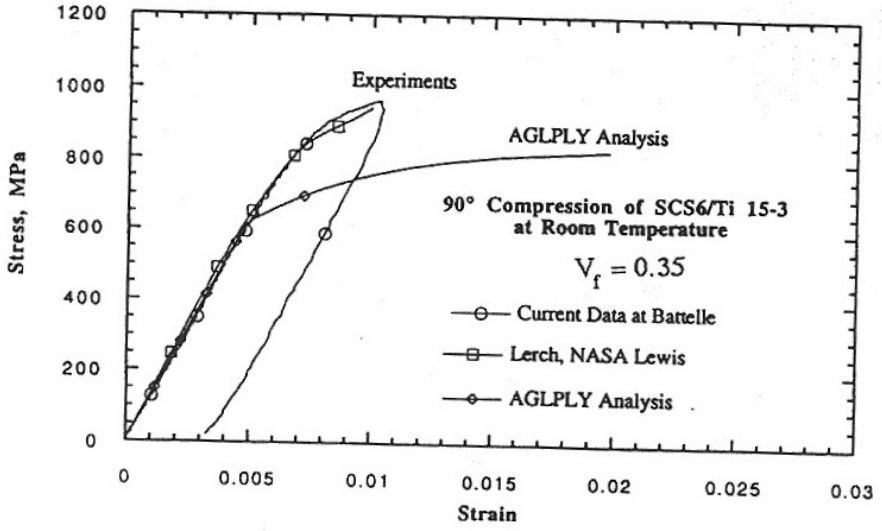

Figure 6. AGLPLY analysis results for $[90]_8$ stress-strain response in compression.

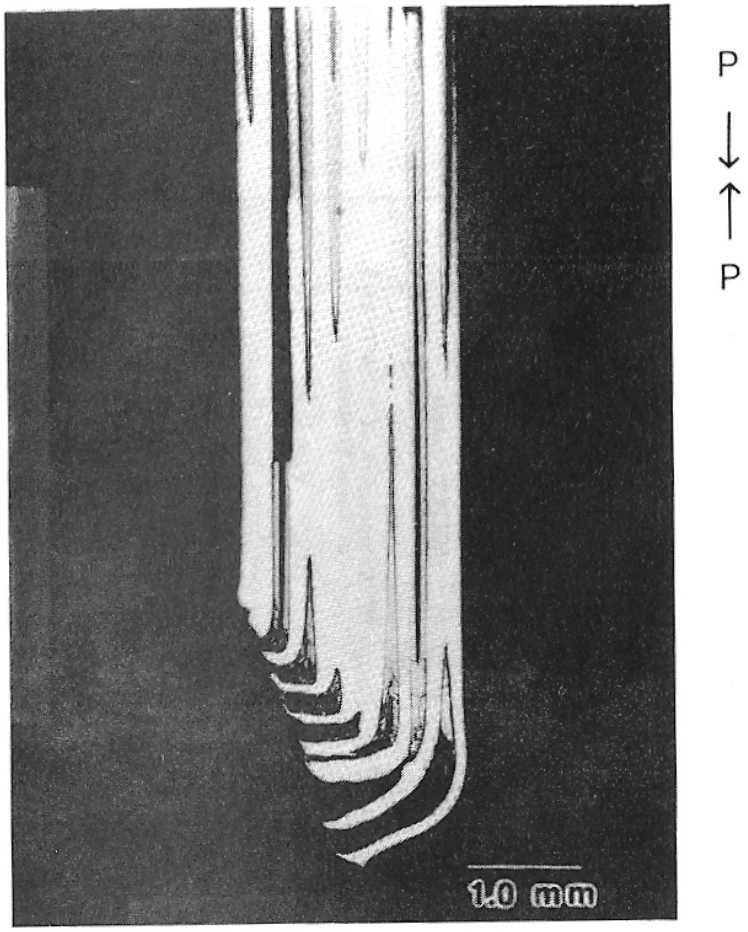

Figure 7. Fiber buckling in $[0]_8$ lamina in compression at RT.

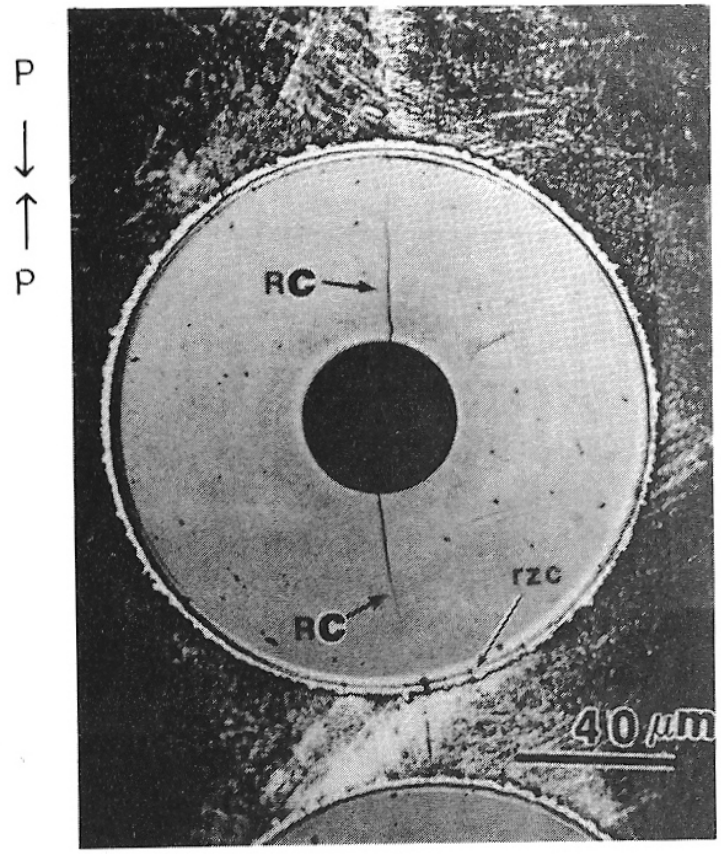

Figure 8. Radial cracks in SCS-6 fiber in a $[90]_8$ Ti 15-3/SCS-6, lamina under compression at room temperature. Loading is up and down.

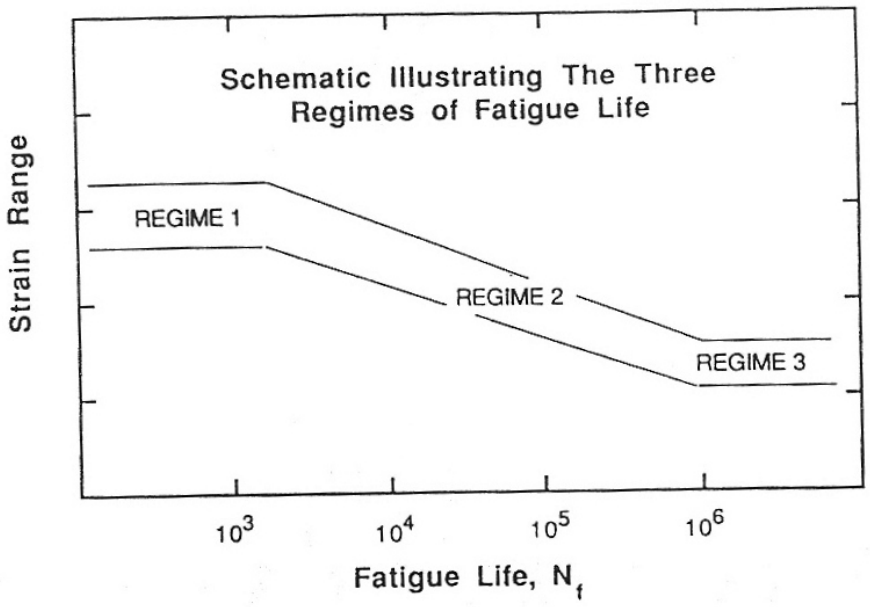

Figure 9. Three regimes of composite fatigue.

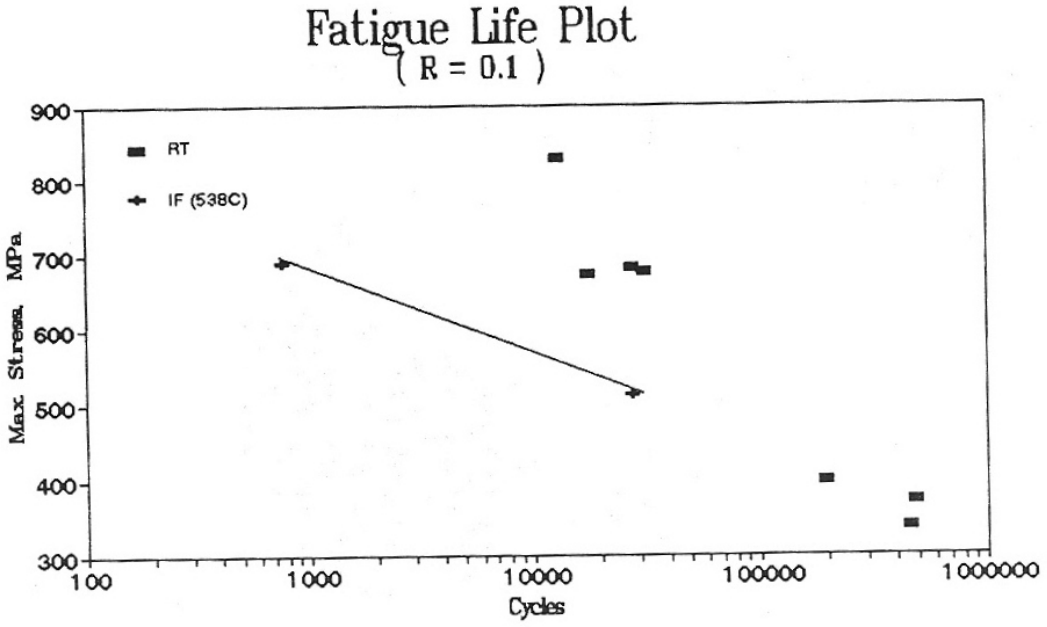

Figure 10. Room temperature fatigue life plot for 15 vol % SCS-6/Ti 15-3 MMC

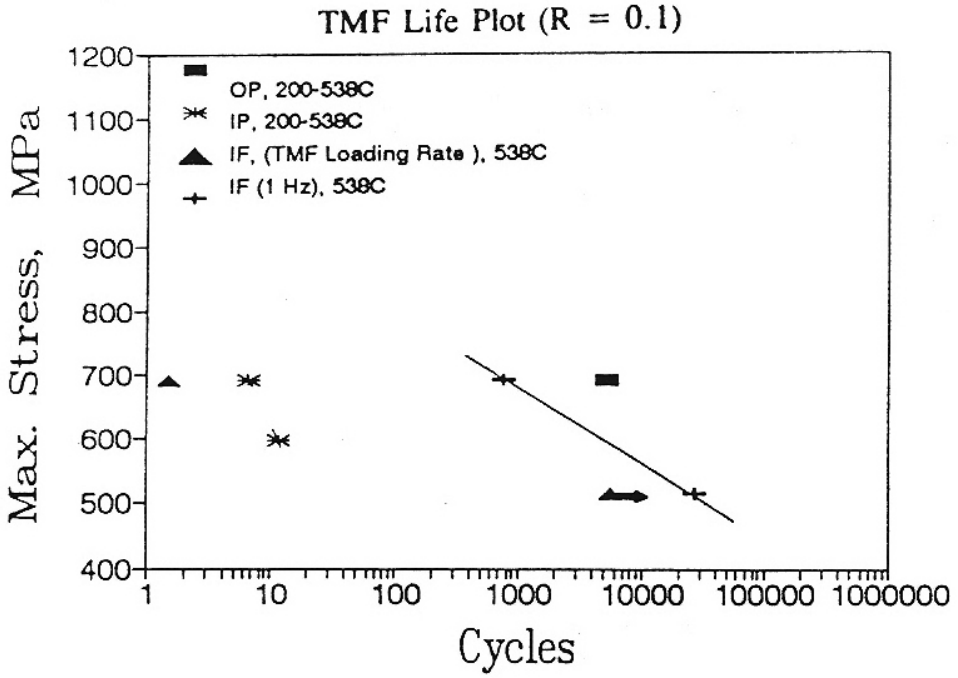

Figure 11. Thermomechanical fatigue (TMF) life plot for 15 vol % SCS-6/Ti 15-3

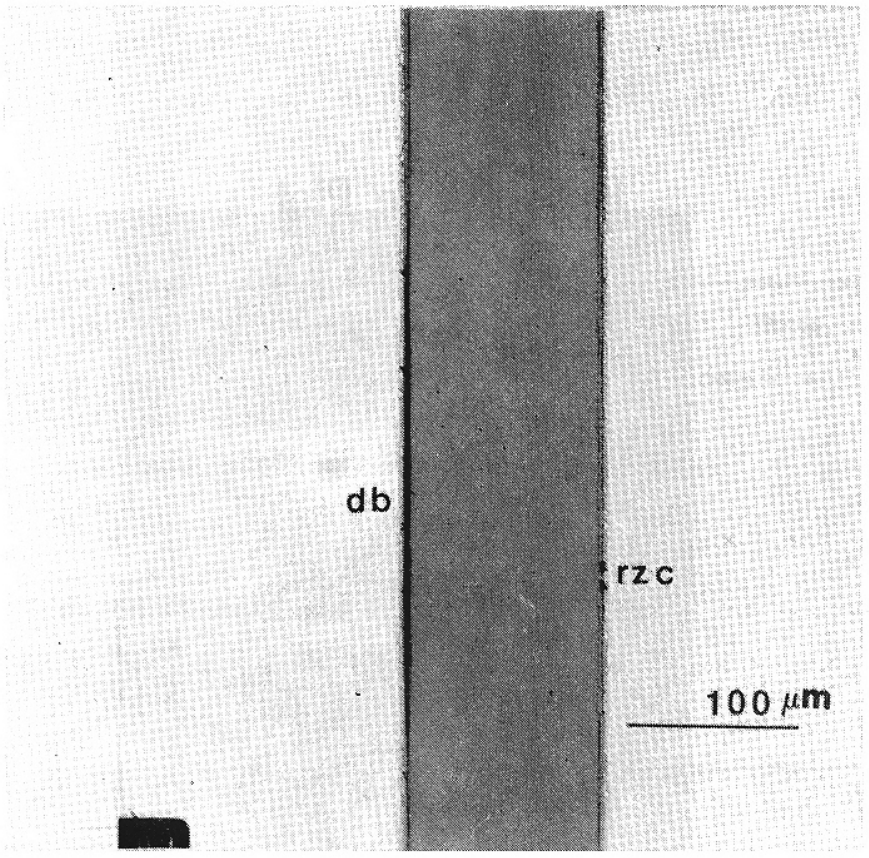

Figure 12. Isothermal fatigue specimen (max. stress: 690 MPa, R=0.1, T=538 C) showing fiber-matrix debonding (db) and reaction zone cracking (rzc).

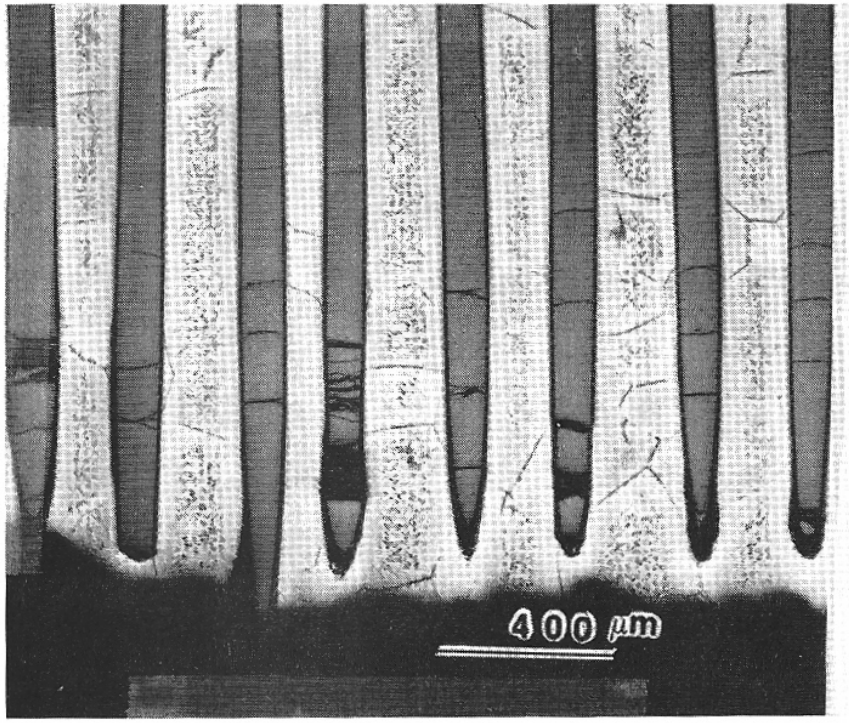

Figure 13. In-phase TMF specimen (max. stress range: 690 MPa, R=0.1, temperature cycle: 200-538 C) showing fiber fracture which are localized and absence of matrix cracking.

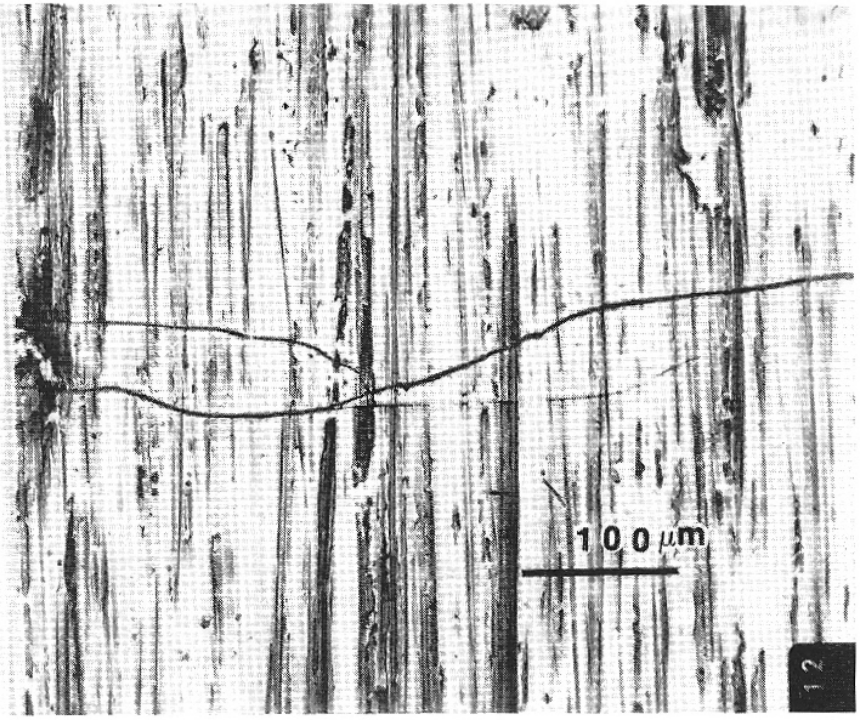

Figure 14. Out-of-phase TMF (max. stress: 690 MPa, R=0.1, temperature cycle = 200-538 C) showing surface matrix cracking.